Decreased fast time-scale spectral diffusion of a non-polar InGaN quantum dot

Claudius Kocher,[†] John C. Jarman,[‡] Tongtong. Zhu,[‡] Gunnar Kusch,[‡] Rachel. A. Oliver,[‡] and Robert A. Taylor*,[†]

†*Department of Physics, University of Oxford, Parks Road, Oxford OX1 3PU, U.K.*
‡*Department Materials Science and Metallurgy, University of Cambridge, 27 Charles Babbage Road, Cambridge CB3 0FS, U.K.*

E-mail: robert.taylor@physics.ox.ac.uk

Abstract

Spectral diffusion can lead to considerable broadening of the linewidth of nitride quantum dots. Here, InGaN quantum dots grown on a non-polar plane were shown to exhibit a decreased spectral diffusion rate compared to polar nitride dots. A robust intensity correlation method was used to measure the spectral diffusion rate of six quantum dots. A maximum spectral diffusion time of 1170 ± 50 ns was found. An increase of the rate with increasing power was observed. The decreased internal field leads to a lifetime for the non-polar dots that is shorter than that for polar dots, the important ratio of spectral diffusion time to lifetime is more favorable for non-polar quantum dots, thereby increasing the chances of generating indistinguishable photons.

Keywords

quantum dot, nitride, single photon, spectral diffusion

Introduction

The performance of semiconductor quantum dots (QDs) is getting ever closer to the characteristics of an ideal single-photon source. Experiments based on arsenide QDs demonstrated high single-photon purity,[1] high source efficiency,[2] high indistinguishability,[3] and even the efficient generation of entangled-photon pairs.[4] Whilst arsenide QDs need to be operated at cryogenic temperatures, nitride QDs have been demonstrated to emit single photons at elevated temperatures –up to 350 K– due to larger exciton binding energies and larger band offsets.[5–9] However, the emission lines of nitride dots are commonly inhomogeneously broadened by at least a factor of 100 compared to their lifetime limit,[10,11] which ultimately limits their indistinguishability. The broadening is caused by spectral diffusion, an effect generated by trapping and untrapping of charge carriers close to a dot generating a changing local electric field. This leads, via the quantum confined Stark effect (QCSE), to changes in the emission energy of the dot. This effect is stronger for nitride QDs than for arsenide QDs, as firstly the strong polar nature of nitride materials results in large permanent dipoles for excitons in nitride QDs, thereby increasing the coupling to the electrostatic environment and amplifying the strength of spectral diffusion.[12] Secondly, growth methods for nitride dots have had less time to be refined when compared to arsenide dots, and they also exhibit increased point defect and dislocation densities, which can act as traps for the carriers.[13–15] Spectral diffusion presents the largest obstacle for the generation of highly indistinguishable photons with nitride dots, al-

though other sources of decoherence may exist, such as phonon interactions.[16]

Here, we investigate a route to reduce the impact of spectral diffusion by using InGaN QDs grown on a *non-polar* plane. Although they are not fully free of an internal electric field, the area facing the polar direction is much reduced due to their small height-to-diameter ratio, thus leading to a reduced in-built potential, as indicated by $\mathbf{k} \cdot \mathbf{p}$ simulations, and a decreased average lifetime by an approximate factor of 10 found in microphotoluminescence (μPL) studies.[17,18] Additionally, a high degree of linearly polarization is seen in the emission spectra, aligned to a crystal direction due to an anisotropic strain distribution inherent in the non-polar QD growth.[19,20] This property is crucial for the encoding of information in free-space quantum communication protocols.[21,22]

The impact of spectral diffusion can be seen in the changes in the QD peak emission energy over the course of a few minutes. This is shown for the dot presented in Figure 1. Although the emission line appears to be stable over five minutes in the colour-representation, fitting each spectrum with a Gaussian reveals that although the emission energy is remarkably stable for a nitride quantum dot, variations in the peak emission energy by $\sim 20\,\mu$eV are still present. The variations observed in Figure 1 occur on a timescale of several seconds, however, there is also spectral diffusion occurring on a much faster timescale, and it is this which crucially limits the indistinguishability. Unfortunately timescales below a few milliseconds are not amenable to time-integrating spectral methods. Therefore, previous reports employed a hole-burning technique[23] or intensity correlation measurements in combination with resonant excitation.[24,25] The most comprehensive method is photon correlation interferometry which offers simultaneously high spectral and time resolution. It has been used for the investigation of spectral diffusion in GaAs QDs, NV centers in diamond, colloidal CdSe/CdS QDs, defect emission in BN and colloidal lead halide perovskite QDs.[26–30] The last three reports were able to identify the dominant spectral diffusion mechanism as random jumps with a constant rate with a Gaussian envelope in contrast to a continuous spectral change. However, the experimental setup for this method requires good stability and precise alignment of a Michelson interferometer, along with a high QD brightness because of the losses caused by a larger number of optical elements.

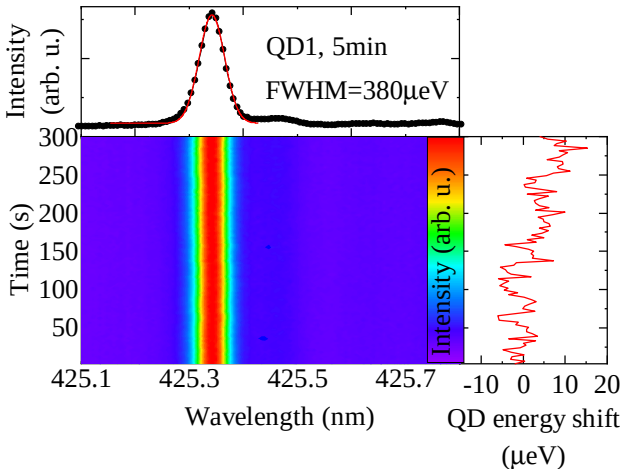

Figure 1: Colour-coded emission spectra of QD1 taken every 3 s over 5 min, taken with the third diffraction order of the 1200 l/mm grating at an excitation power density of $10\,\mathrm{kWcm^{-2}}$. Top: Sum of all spectra. A Gaussian fit extracts a FWHM of $380\,\mu$eV. Right: Shift of the QD peak energy over the course of 5 min, extracted with a Gauss fit to each spectrum.

Since the brightness of nitride dot devices is still modest, given that the development of highly efficient cavities is still in its infancy,[31–33] and because resonant excitation is yet to be demonstrated for nitride dots, the only two dedicated reports on fast timescale spectral diffusion in nitride QDs used another robust intensity correlation technique first demonstrated with a CdSe/ZnSe QD.[34] It consists of measuring the second order correlation function with a Hanbury Brown and Twiss (HBT) setup while spectrally selecting only a part of the inhomogeneously broadened QD line. This means that for some time, the homogeneous line remains in this spectral detection window during which the local charge landscape around the QD does not change significantly. When it does, the line will eventually jump out of the detection window and then continues to jump randomly in and

out over time. This leads to packets of closely spaced photons separated in time entering the HBT setup and results in a bunching peak at short delay times in the HBT measurement trace, in addition to the photon anti-bunching dip. It has been established that the width of the spectral detection window does not influence the measured spectral diffusion bunching decay time; only the bunching amplitude increases with a narrower detection width.[34]

There are two reports dedicated to the measurement of fast timescale spectral diffusion of nitride dots, both at 4 K. The study of an interface fluctuation GaN/AlGaN QD yielded a maximum spectral diffusion time of 22 ns,[35] whereas a study of an InGaN/GaN dot in a distributed Bragg reflector cavity reported a maximal spectral diffusion time of 340 ns.[16] Both agreed with previous studies that the spectral diffusion time is inversely proportional to the laser excitation power at low power,[27,36] since it results in a higher charge carrier density close to the dot, thereby leading to faster changes in the electric environment. For the InGaN dot, despite a 10 times higher excitation power density, the spectral diffusion time was longer than that for the GaN dots; this was tentatively attributed to deeper traps.[16] Recently, a study of an InGaN/GaN QD buried in a photonic horn structure included a similar measurement, yielding a spectral diffusion time of 140 ns (at an excitation power of $0.12 \cdot P_{\mathrm{sat}} = 0.5\,\mathrm{Wcm}^{-2}$) at 4 K. The horn structure lead to a reduction of the excitation power density by several orders of magnitude through concentration of the laser excitation. Another recent study on room-temperature emission of GaN/AlN QDs grown on a Si substrate mentioned a much reduced maximum spectral diffusion time of 15 ns as a by-product of an HBT measurement of a QD line.[37] The factor leading to the strong spectral diffusion time decrease is likely to be the temperature: at 300 K the thermal energy available is much higher than that at 4 K enabling charge carriers to escape from traps more easily. All previous results are summarised in Figure 6.

A factor common to all these measurements is that the QDs were grown on a polar crystal plane, enhancing the sensitivity to changes in the electric environment. Here, we investigate fast spectral diffusion in nitride QDs grown on a non-polar plane. Theoretical studies have shown that for a-plane QDs, second-order piezoelectricity can cancel a significant fraction of the built-in potential induced by first-order piezoelectricity and spontaneous polarization.[38] One therefore may expect a reduction in the strength of the spectral diffusion given the reduced internal field. However, the defect density in non-polar nitride material is currently found to be larger, increasing the strength of spectral diffusion. We shall see that most investigated QDs show longer spectral diffusion times at 4 K, underlining the importance of the reduction in internal electric fields.

Results and discussion

The overall emission spectrum from the sample is broad, with InGaN-related emission observable at wavelengths ranging from 390 nm - 500 nm. Microphotoluminescence maps of the emission in this spectral region (see, as an example, figure 2(a) which shows the emission at 444 nm - 452 nm) show a regular pattern of parallel stripes oriented along $[1\bar{1}00]$. (The approximate crystal axis orientation is obtained from an optical micrograph of the sample: visible striations on the surface extend along [0001].[39]) This is due to an epitaxial layer overgrowth (ELOG) step during the growth used to reduce the density of threading dislocations[39,40] (see Methods). Stripes of SiO_2 were employed to block vertical growth of GaN and lateral overgrowth was promoted through a lower pressure and V-III ratio. Within the bright stripes seen in μPL maps of the InGaN luminescence, more intense spots can be observed, which correlate with the locations of sharp quantum dot emission peaks identified by automated dot location software. Similarly, bright cathodoluminescence (CL) excited by the electron beam in a scanning electron microscope (SEM) arising from the InGaN layer can be observed in stripes across the sample. (See, as an example, figure 2(c), which shows the emission at 400 nm - 480 nm). In the secondary electron (SE) im-

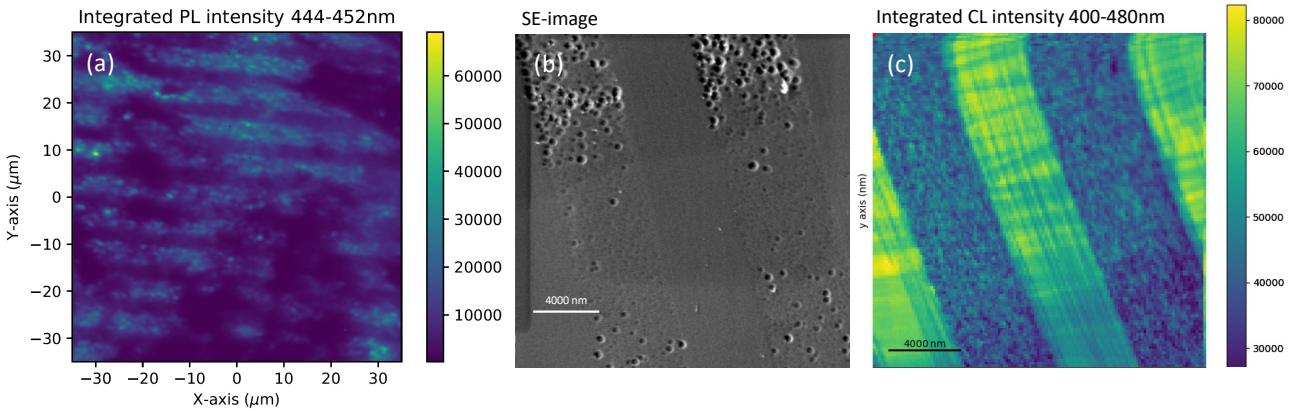

Figure 2: (a) Microphotoluminescence map for wavelengths from 444 to 452 nm in which the luminescence arising from the InGaN demonstrates bright bands on which quantum dot (QD) emission shows up as intense spots. (b) In this secondary electron (SE) image, window regions of high defect density are rough, whereas window regions are smoother. (c) In a cathodoluminescence map of the same area, we see that the bright InGaN emission (here integrated from 400 to 480 nm) arises from the low defect density wing regions, suggesting that QD emission comes predominately from these low defect density areas.

age (Figure 2(b)), we can also identify the high and low defect density regions of the underlying GaN pseudo-substrate grown by the ELOG method.[39,40] The high defect density "window" regions, exhibit a rough surface topography with many pits, relating to the termination of threading dislocations. In the CL, these regions exhibit a lower intensity of InGaN-related emission. The low defect density "wing" regions exhibit a smoother topography, and the CL shows brighter InGaN emission, although narrow dark bands parallel to edges of the wing can be observed, which relate to the presence of extended basal plane stacking faults. We have not been able to identify QD signatures in CL from this specific sample, for reasons which remain unclear. However, the correlation of the high intensity InGaN emission with the low defect density region in the SE-image, and with the QD locations in μPL suggests that the majority of the bright QDs seen in PL are in the low defect density wing region. This is perhaps unsurprising, since carrier recombination at defects provides an alternative non-radiative recombination pathway, leading to reduced radiative recombination.

The brightest dot found through microPL mapping was chosen for a detailed study. Its spectrum is presented in Figure 1. It features a low QW background, important for a spectral diffusion measurement with good signal-to-noise ratio. Its saturation power of $P_{\mathrm{sat}} = 30 \pm 3\,\mathrm{kWcm}^{-2}$ under CW excitation (see Fig. S2(a)) is much higher than in the previously mentioned nitride dot studies (at 4 K). This is partially because here no cavity was used in contrast to the previous InGaN reports. The saturation intensity is $I_{\mathrm{sat}} = 740 \pm 30$ photons/s, the lifetime is 387 ± 3 ps (Fig. S1(b)) and the estimated collection efficiency is 1%, resulting in a net out-coupling efficiency of 3%, which is reasonable for a QD emitting in a micropillar without a cavity. The dot linewidth increases linearly with rising power, with a width of about 310 μeV interpolated to zero excitation power (Fig. S1(a)). This is another indication of fast-timescale spectral diffusion.

The single photon nature of the QD emission was confirmed using a second order correlation function was measured with an HBT setup, choosing a broad spectral window of 2 meV to include the entire inhomogeneously broadened line over the whole measurement time of several hours. The ratio of the QD PL to the

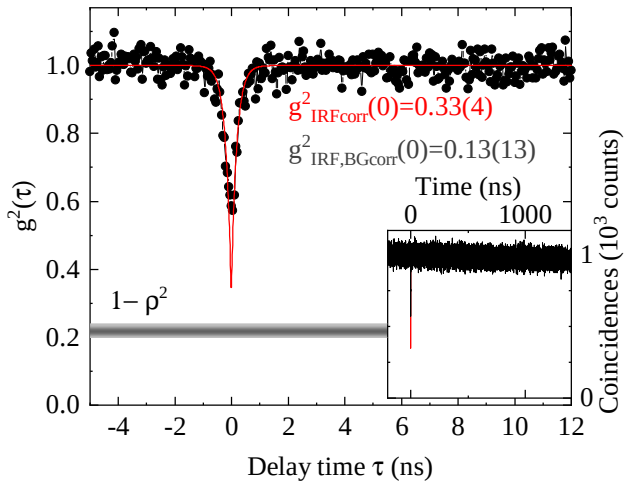

Figure 3: Second order correlation function of the emission of QD1 measured with a wide spectral filter window of 2meV, which included the whole QD line. Excitation power density $2.9\,\mathrm{kWcm}^{-2} = 0.1 \cdot P_{\mathrm{sat}}$. The inset shows the whole HBT trace, expanded over 1 μs. The decrease of the coincidence count level is due to pile-up, which is explained in the main text and the supporting information.

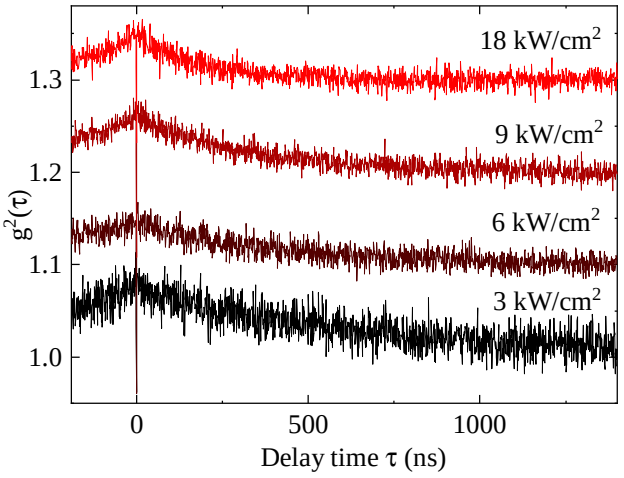

Figure 4: Second order correlation function of the emission of QD1 measured as a function of excitation power with a narrow spectral filter window of 1 meV centred on the lower energy halve of the QD emission line. The top three traces are shifted by 0.1 each. Every HBT trace was corrected for the pile-up decay and normalised, as described in detail in the Supporting Information. A distinct bunching effect can be observed in addition to the anti-bunching dip at zero delay.

whole signal was $\rho = 0.88 \pm 0.04$. The HBT trace shown in Figure 3 features a dip at zero delay, which yields a second order correlation value of $g^2_{\mathrm{IRF,BGcorr}}(0) = 0.13 \pm 0.13$ after correction firstly for the instrument response function[41] and then secondly the QW background emission.[5,7] It therefore proves that the QD line emits single photons. More importantly for this study, the same HBT trace viewed on a larger scale shown in the inset of Figure 3 exhibits no longer-timescale bunching, which indicates the absence of blinking or random charging events of the QD.

However, a visible feature is the slight reduction of the coincidence counts with increasing delay time. This is a measurement artefact arising due to the start-stop mode of HBT measurement which was employed. It is referred to as "pile up": the longer the delay time, the more likely it is that a photon detection event resets the clock, leading to an exponential decay of the coincidence counts. Its electronic origin is also indicated by the fact that the decay starts at the left of the trace. It has been accounted for by measuring the decay time at different photon detection rates (Fig. S2(a)), showing a decreasing pile-up decay time for an increased photon detection rate, and then by fitting the data with a power law (Fig. S2(b)). This allows us to correct the data taken in the following spectral diffusion HBT measurements for the pileup, details are found in the Supporting Information. Another HBT measurement mode called time-tagged would have been more appropriate, but the start-stop mode yields similar results as demonstrated with a comparison measurement shown in Fig. S4.

Next, the spectral selection window was reduced to about half the QD's linewidth and an HBT measurement was carried out at different excitation powers. Four example HBT traces are shown in Figure 4, corrected for the pile-up. They have been rebinned with a bin width of 1 ns to increase the signal-to-noise ratio, therefore the antibunching dip is almost averaged out. In contrast, the bunching caused by the spectral diffusion is clearly visible. It can be seen that each trace exhibits a longer

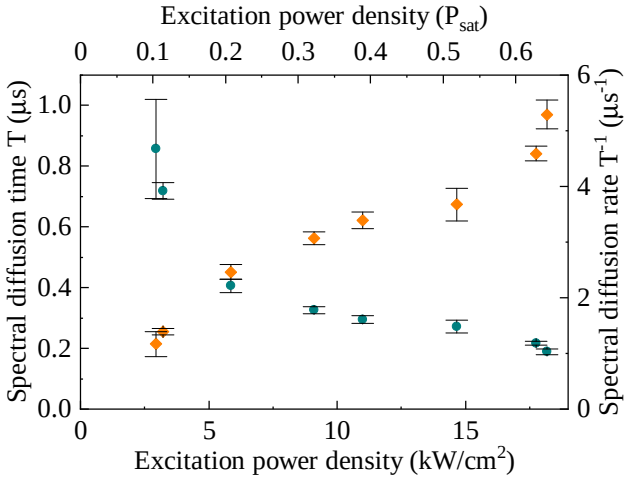

Figure 5: Excitation power dependence of the spectral diffusion time (left axis and green dots) and its inverse, the spectral diffusion rate (right axis and orange diamonds) for QD1.

bunching decay: the bunching decay time increases with decreasing excitation power. This is because lower excitation power means fewer excited charge carriers which could change the electric environment of the QD. To see this relationship more clearly, the trace was fitted with the equation

$$g^2(\tau) = 1 + B \cdot \mathrm{e}^{-|\tau|/T} \qquad (1)$$

with the spectral diffusion (bunching) time T and amplitude B,[16,35] neglecting the few data points contributing to the anti-bunching dip. The results are shown in Figure 5, where the dependence of the inverse of the spectral diffusion time, the spectral diffusion rate, on the excitation power density is shown. A linear trend can be seen, going through the origin, indicating that the spectral diffusion is entirely laser-induced, in agreement with most other reports.[27,35,36] The longest measured spectral diffusion time for this dot is 860 ± 160 ns. It should be noted that for higher excitation power a square root power dependence would be observed.[37]

To determine whether this is not just one QD with an exceptionally stable electric environment, but that the grown plane of the QDs has a significant effect on the spectral diffusion for all dots, the measurement was repeated for several QDs, solely chosen for their brightness. It should be noted that previous reports just focused on a single dot. All measured spectral diffusion rates, including those of all previous reports, are shown in Figure 6 as a function of excitation power. It can be seen that most of the non-polar QDs exhibit lower spectral diffusion rates than the previous studies on polar GaN and InGaN QDs. Notably, based on the lowest measured rate, the longest spectral diffusion time amounted to 1170 ± 50 ns which is more than 3 times longer than the longest time previously reported. This suggests that non-polar nitride dots are better suited to potentially produce photon with a high indistinguishability than polar ones. It should also be noted that these QDs were predominately located in the wing region of an ELOG sample, so a reduced density of dislocations may have contributed to the observed long spectral diffusion times. The wing region does, however, still contain a significant density of extended defects, in the form of basal plane stacking faults, so defect-related carrier trapping is still likely to influence QD performance, suggesting that the non-polar nature of the material is the predominate factor causing the improvement. Furthermore, non-polar QDs exhibit significantly shorter lifetimes, thereby increasing further the ratio of the spectral diffusion time to the lifetime, which is equivalent to the number of potential operations in quantum metrology or quantum computing processes, for example the generation of cluster states.[42]

It should be noted that, although the setup was not optimised for polarization measurements due to the large number of mirrors and use of a dichroic mirror leading to wavelength dependent polarization scrambling, for one QD with a spectral diffusion time of 150 ns a high polarization degree of 96% could be measured. Its axis was aligned along the m-crystal direction due to anisotropic strain in the growth plane, as for the vast majority of dots found in a previous study.[20] Therefore it does not belong to the minority of dots emitting orthogonally polarized photons (most likely due to a strong base asymmetry[20]), therefore it is unlikely that the long spectral diffusion times are linked to this small subset of dots.

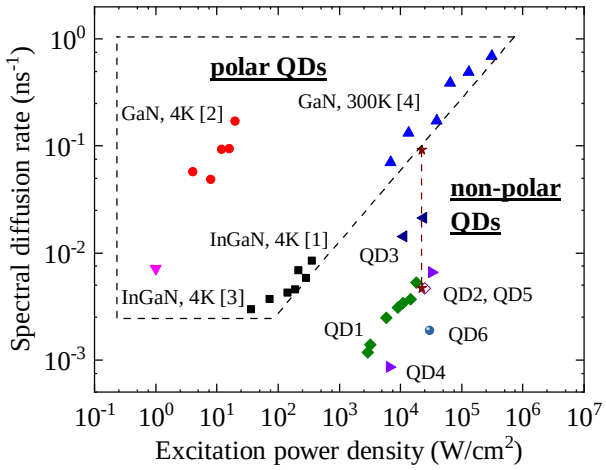

Figure 6: Overview of the spectral diffusion rate as a function of excitation power density for all measured QDs in this study. The results of previous reports on polar nitride dots are also included. QD2 exhibited a biexponential bunching decay, see Fig. S4.

Conclusion We presented measurements of the spectral diffusion time of 6 non-polar InGaN dots, employing a robust intensity correlation method. The majority of these QDs exhibited similar and longer spectral diffusion times than those in all previous reports on nitride dots, which used polar material. Along with the significantly shorter lifetimes due to the reduction of the strength of the QCSE, non-polar QDs are in a better position to achieve high indistinguishability values. To make such measurements feasible, the employment of cavities[32] would be needed to boost the out-coupling efficiency. An additional benefit would be the reduction of the saturation power and thereby of the strength of spectral diffusion. It will also be necessary to improve the growth recipes to reduce the defect density and eliminate the spectral overlap between QD and QW emission.

Methods

Fabrication

The QDs were grown via metal-organic chemical vapour deposition with a method called modified droplet epitaxy (see details in[39]). The template was prepared with epitaxial lateral overgrowth in order to reduce the dislocation density in some areas. A 100 nm layer of SiO_2 was grown on top of an as-grown *a*-plane GaN template and etched into 5 μm-wide stripes separated by 5 μm. GaN growth was again carried out under a pressure of 100 Torr and a V/III ratio of 60 at 1050 °C, favoring lateral growth until full coalescence was achieved. Another GaN buffer was grown with a V/III ratio of 740 before the QD growth step and the final capping. Then, the sample was dry-etched into 180 nm wide and 500 nm long pillars using randomly dispersed SiO_2 spheres as etching mask.

Photoluminescence

The sample was held at 4 K in a closed-cycle cryostat (attoDRY800) on a translational piezo positioner cube with 3 axes (ANPx/z101, *Attocube*). The sample was non-resonantly excited via the InGaN QW by means of a continuous wave laser with a wavelength of 405 nm. A 4f-scanning setup was used to obtain PL maps of the size of approximately $100 \times 100\,\mu m^2$ to search with a program automatically for bright QDs. This allowed identification of brightly emitting QWs in order to shorten the measurement time (which depends quadratically on the QD intensity). It also allowed the recording of microphotoluminescence maps (typically $70 \times 80\,\mu m^2$ in size) for various wavelength bands. The laser was focused on the sample with a 100× objective with a numerical aperture of 0.7 (M Plan Apo infinity corrected, *Mitutoyo*), resulting in an approximate spot diameter on the sample of 1 μm. The PL was collected through the same objective, separated from the excitation laser by a dichroic mirror (Di02-R405-25x36, *Semrock*) and coupled into a multimode fibre. The coupling lens and fibre diameter were chosen such that the corresponding spot on the sample had a diameter of approximately 1μm. The fibre was directly coupled into a spectrometer with a 0.5 m focal length (Shamrock 500i, *Andor*), equipped with two 1200 l/mm gratings with blaze angles optimized for 500 nm and 1000 nm, and a thermoelectrically cooled charge-coupled device. The setup had a resolution of 820 μeV at 425 nm,

the use of third diffraction order improved this by approximately a factor of 3. For the second order correlation measurements, the spectrometer was used as an adjustable filter. The HBT setup consisted of a non-polarizing 50:50 beamsplitter and two photomultiplier tubes (PMTs, H10720, *Hamamatsu*) and was located directly at the second output of the spectrometer. The PL was refocused onto the PMTs with a biconvex lens. To account for drift during the HBT measurements, a LabView program was used to optimise the PL intensity by adjusting the sample position in regular time intervals. The signals from the PMTs were processed by a time correlation single photon counting card in start-stop mode (TimeHarp260, *PicoQuant*). For the time-tagged measurement, a PicoHarp 300 was used. A Python script using C libraries was used to analyse the time-tagged data.[43] For the lifetime measurement of QD1, a frequency-doubled Titanium-Sapphire laser at 405 nm with an approximate pulse width of 100 fs was used to excite the dot. One PMT of the HBT setup was used along with a fast sync diode and the TimeHarp260 card.

Cathodoluminescence

To compare the locations of the bright InGaN luminescence related to the QDs to the locations of high and low defect density regions of the sample, cathodoluminescence hyperspectral maps were acquired at 10 K using a *Attolight* Allalin 4027 Chronos dedicated CL scanning electron microscope. CL spectra and images were recorded with an iHR320 spectrometer with a focal length of 320 mm. Measurements were performed with a 150 l/mm grating blazed at 500 nm, or a 600 l/mm grating blazed at 350 nm, and an *Andor* 1024 pixel charged coupled device. Grating and slit width were adjusted to provide the best compromise between resolution and intensity for each of the measurements. The monochromatic image was extracted from the hyperspectral dataset using the HyperSpy multi-dimensional data analysis toolbox.[44]

Supporting information

The supporting information shows the power dependence and lifetime of QD1, and discusses pileup correction in the HBT traces. This material is available free of charge via the internet at http://pubs.acs.org.

Acknowledgement
This work was funded by the EPSRC (grant EP/M012379/1). The authors would like to thank Florian LeRoux for help to get the Python code running.

References

(1) Hanschke, L.; Fischer, K. A.; Appel, S.; Lukin, D.; Wierzbowski, J.; Sun, S.; Trivedi, R.; Vučković, J.; Finley, J. J.; Müller, K. Quantum Dot Single Photon Sources with Ultra-Low Multi-Photon Probability. *npj Quantum Inf.* **2018**, *4*, 2056.

(2) Somaschi, N. et al. Near-Optimal Single-Photon Sources in the Solid State. *Nat. Photonics* **2016**, *10*, 340.

(3) Schöll, E.; Hanschke, L.; Schweickert, L.; Zeuner, K. D.; Reindl, M.; Covre Da Silva, S. F.; Lettner, T.; Trotta, R.; Finley, J. J.; Müller, K.; Rastelli, A.; Zwiller, V.; Jöns, K. D. Resonance Fluorescence of GaAs Quantum Dots with Near-Unity Photon Indistinguishability. *Nano Lett.* **2019**, *19*, 2404.

(4) Wang, H. et al. On-Demand Semiconductor Source of Entangled Photons Which Simultaneously Has High Fidelity, Efficiency, and Indistinguishability. *Phys. Rev. Lett.* **2019**, *122*, 1–6.

(5) Puchtler, T. J.; Wang, T.; Ren, C. X.; Tang, F.; Oliver, R. A.; Taylor, R. A.; Zhu, T. Ultrafast, Polarized, Single-Photon Emission from m-Plane InGaN Quantum Dots on GaN Nanowires. *Nano Lett.* **2016**, *16*, 7779.

(6) Wang, T.; Puchtler, T. J.; Zhu, T.; Jarman, J. C.; Nuttall, L. P.; Oliver, R. A.; Taylor, R. A. Polarisation-Controlled Single Photon Emission at High Temperatures from InGaN Quantum Dots. *Nanoscale* **2017**, *9*, 9421.

(7) Holmes, M. J.; Choi, K.; Kako, S.; Arita, M.; Arakawa, Y. Room-Temperature Triggered Single Photon Emission from a III-Nitride Site-Controlled Nanowire Quantum Dot. *Nano Lett.* **2014**, *14*, 982.

(8) Holmes, M. J.; Kako, S.; Choi, K.; Arita, M.; Arakawa, Y. Single Photons from a Hot Solid-State Emitter at 350 K. *ACS Photonics* **2016**, *3*, 543.

(9) Patra, S. K.; Schulz, S. Exploring the Potential of c-Plane Indium Gallium Nitride Quantum Dots for Twin-Photon Emission. *Nano Lett.* **2020**, *20*, 234–241.

(10) Arita, M.; Le Roux, F.; Holmes, M. J.; Kako, S.; Arakawa, Y. Ultraclean Single Photon Emission from a GaN Quantum Dot. *Nano Lett.* **2017**, *17*, 2902.

(11) Cho, J.-H.; Kim, Y. M.; Lim, S.-H.; Yeo, H.-S.; Kim, S.; Gong, S.; Cho, Y.-H. Strongly Coherent Single Photon Emission from Site-Controlled InGaN Quantum Dots Embedded in GaN Nano-Pyramids. *ACS Photonics* **2017**, *5*, 439–444.

(12) Kindel, C.; Callsen, G.; Kako, S.; Kawano, T.; Oishi, H.; Hönig, G.; Schliwa, A.; Hoffmann, A.; Arakawa, Y. Spectral Diffusion in Nitride Quantum Dots: Emission Energy Dependent Linewidths Broadening Via Giant Built-in Dipole Moments. *Phys. Status Solidi RRL* **2014**, *8*, 408–413.

(13) Gurioli, M.; Wang, Z.; Rastelli, A.; Kuroda, T.; Sanguinetti, S. Droplet Epitaxy of Semiconductor Nanostructures for Quantum Photonic Devices. *Nat. Mater.* **2019**, *18*, 799–810.

(14) Gibart, P. Metal Organic Vapour Phase Epitaxy of GaN and Lateral Overgrowth. *Rep. Prog. Phys.* **2004**, *67*, 667–715.

(15) Reid, B. P. L.; Zhu, T.; Puchtler, T. J.; Fletcher, L. J.; Chan, C. C. S.; Oliver, R. A.; Taylor, R. A. Origins of Spectral Diffusion in the Micro-Photoluminescence of Single InGaN Quantum Dots. *Jpn. J. Appl. Phys.* **2013**, *52*, 08JE01.

(16) Gao, K.; Springbett, H.; Zhu, T.; Oliver, R. A.; Arakawa, Y.; Holmes, M. J. Spectral Diffusion Time Scales in InGaN/GaN Quantum Dots. *Appl. Phys. Lett.* **2019**, *114*, 112109.

(17) Patra, S. K.; Wang, T.; Puchtler, T. J.; Zhu, T.; Oliver, R. A.; Taylor, R. A.; Schulz, S. Theoretical and Experimental Analysis of Radiative Recombination Lifetimes in Nonpolar InGaN/GaN Quantum Dots. *Phys. Status Solidi B* **2017**, *254*, 1600675.

(18) Reid, B. P. L.; Zhu, T.; Chan, C. C. S.; Kocher, C.; Oehler, F.; Emery, R.; Kappers, M. J.; Oliver, R. A.; Taylor, R. A. High Temperature Stability in Non-Polar $(11\bar{2}0)$ InGaN Quantum Dots: Exciton and Biexciton Dynamics. *Phys. Status Solidi C* **2014**, *11*, 702.

(19) Reid, B. P. L.; Kocher, C.; Zhu, T.; Oehler, F.; Chan, C. C. S.; Oliver, R. A.; Taylor, R. A. Non-Polar InGaN Quantum Dot Emission with Crystal-Axis Oriented Linear Polarization. *Appl. Phys. Lett.* **2015**, *106*, 171108.

(20) Wang, T.; Puchtler, T. J.; Patra, S. K.; Zhu, T.; Ali, M.; Badcock, T. J.; Ding, T.; Oliver, R. A.; Schulz, S.; Taylor, R. A. Direct Generation of Linearly Polarized Single Photons with a Deterministic Axis in Quantum Dots. *Nanophotonics* **2017**, *6*, 1175.

(21) Bennett, C. H.; Brassard, G. Quantum Cryptography: Public Key Distribution

and Coin Tossing. Proc. IEEE Int. Conf. Comput. Syst. Signal Process. Bangalore, India, 1984; p 175.

(22) Tang, Z.; Liao, Z.; Xu, F.; Qi, B.; Qian, L.; Lo, H.-K. Experimental Demonstration of Polarization Encoding Measurement-Device-Independent Quantum Key Distribution. *Phys. Rev. Lett.* **2014**, *112*, 190503.

(23) Palinginis, P.; Tavenner, S.; Lonergan, M.; Wang, H. Spectral Hole Burning and Zero Phonon Linewidth in Semiconductor Nanocrystals. *Phys. Rev. B* **2003**, *67*, 201307.

(24) Jahn, J. P.; Munsch, M.; Béguin, L.; Kuhlmann, A. V.; Renggli, M.; Huo, Y.; Ding, F.; Trotta, R.; Reindl, M.; Schmidt, O. G.; Rastelli, A.; Treutlein, P.; Warburton, R. J. An Artificial Rb Atom in a Semiconductor with Lifetime-Limited Linewidth. *Phys. Rev. B* **2015**, *92*, 245439.

(25) Nawrath, C.; Olbrich, F.; Paul, M.; Portalupi, S. L.; Jetter, M.; Michler, P. Coherence and Indistinguishability of Highly Pure Single Photons from Non-Resonantly and Resonantly Excited Telecom C-Band Quantum Dots. *Appl. Phys. Lett.* **2019**, *115*, 023103.

(26) Schimpf, C.; Reindl, M.; Klenovský, P.; Fromherz, T.; Covre Da Silva, S. F.; Hofer, J.; Schneider, C.; Höfling, S.; Trotta, R.; Rastelli, A. Resolving the Temporal Evolution of Line Broadening in Single Quantum Emitters. *Opt. Express* **2019**, *27*, 35290.

(27) Wolters, J.; Sadzak, N.; Schell, A. W.; Schröder, T.; Benson, O. Measurement of the Ultrafast Spectral Diffusion of the Optical Transition of Nitrogen Vacancy Centers in Nano-Size Diamond Using Correlation Interferometry. *Phys. Rev. Lett.* **2013**, *110*, 027401.

(28) Beyler, A. P.; Marshall, L. F.; Cui, J.; Brokmann, X.; Bawendi, M. G. Direct Observation of Rapid Discrete Spectral Dynamics in Single Colloidal CdSe-CdS Core-Shell Quantum Dots. *Phys. Rev. Lett.* **2013**, *111*, 177401.

(29) Spokoyny, B.; Utzat, H.; Moon, H.; Grosso, G.; Englund, D.; Bawendi, M. G. Effect of Spectral Diffusion on the Coherence Properties of a Single Quantum Emitter in Hexagonal Boron Nitride. *J. Phys. Chem. Lett.* **2020**, 1330–1335.

(30) Utzat, H.; Sun, W.; Kaplan, A. E. K.; Krieg, F.; Ginterseder, M.; Spokoyny, B.; Klein, N. D.; Shulenberger, K. E.; Perkinson, C. F.; Kovalenko, M. V.; Bawendi, M. G. Coherent Single-Photon Emission from Colloidal Lead Halide Perovskite Quantum Dots. *Science* **2019**, *363*, 1068–1072.

(31) Jarjour, A. F.; Taylor, R. A.; Oliver, R. A.; Kappers, M. J.; Humphreys, C. J.; Tahraoui, A. Cavity-Enhanced Blue Single-Photon Emission from a Single InGaNGaN Quantum Dot. *Appl. Phys. Lett.* **2007**, *91*, 052101.

(32) Springbett, H. P.; Gao, K.; Jarman, J.; Zhu, T.; Holmes, M.; Arakawa, Y.; Oliver, R. A. Improvement of Single Photon Emission from InGaN QDs Embedded in Porous Micropillars. *Appl. Phys. Lett.* **2018**, *113*, 101107.

(33) Demory, B.; Katcher, A.; Hill, T.; Teng, C. H.; Zhang, C.; Guo, L. J.; Deng, H.; Ku, P. C. Improving the Radiative Efficiency of InGaN Quantum Dots Via an Open Top Cavity. *ACS Photonics* **2017**, *4*, 795–799.

(34) Sallen, G. et al. Subnanosecond Spectral Diffusion Measurement Using Photon Correlation. *Nat. Photonics* **2010**, *4*, 696.

(35) Gao, K.; Solovev, I.; Holmes, M.; Arita, M.; Arakawa, Y. Nanosecond-Scale Spectral Diffusion in the Single Photon Emission of a GaN Quantum Dot Nanosecond-Scale Spectral Diffusion in

the Single Photon Emission of a GaN Quantum Dot. *AIP Adv.* **2017**, *7*, 125216.

(36) Sallen, G.; Tribu, A.; Aichele, T.; André, R.; Besombes, L.; Bougerol, C.; Richard, M.; Tatarenko, S.; Kheng, K.; Poizat, J. P. Subnanosecond Spectral Diffusion of a Single Quantum Dot in a Nanowire. *Phys. Rev. B* **2011**, *84*, 041405.

(37) Tamariz, S.; Callsen, G.; Stachurski, J.; Shojiki, K.; Butté, R.; Grandjean, N. Toward Bright and Pure Single Photon Emitters at 300 K Based on GaN Quantum Dots on Silicon. *ACS Photonics* **2020**, *7*, 1515–1522.

(38) Patra, S. K.; Schulz, S. Electronic and Optical Properties of Polar, Semi- and Non-Polar InGaN QDs: The Role of Second-Order Piezoelectric Effects. *Jpn. J. Appl. Phys.* **2019**, *58*.

(39) Zhu, T.; Oehler, F.; Reid, B.; Emery, R. M.; Taylor, R. A.; Kappers, M. J.; Oliver, R. A. Non-Polar $(11\bar{2}0)$ InGaN Quantum Dots with Short Exciton Lifetimes Grown by Metal-Organic Vapour Phase Epitaxy. *Appl. Phys. Lett.* **2013**, *102*, 698.

(40) Häberlen, M.; Badcock, T. J.; Moram, M. A.; Hollander, J. L.; Kappers, M. J.; Dawson, P.; Humphreys, C. J.; Oliver, R. A. Low Temperature Photoluminescence and Cathodoluminescence Studies of Nonpolar GaN Grown Using Epitaxial Lateral Overgrowth. *J. Appl. Phys.* **2010**, *108*, 033523.

(41) Kocher, C. C.; Puchtler, T. J.; Jarman, J. C.; Zhu, T.; Wang, T.; Nuttall, L.; Oliver, R. A.; Taylor, R. A. Highly Polarized Electrically Driven Single-Photon Emission from a Non-Polar InGaN Quantum Dot. *Appl. Phys. Lett.* **2017**, *111*, 251108.

(42) Istrati, D.; Pilnyak, Y.; Loredo, J. C.; Antón, C.; Somaschi, N.; Hilaire, P.; Ollivier, H.; Esmann, M.; Cohen, L.; Vidro, L.; Millet, C.; Lemaître, A.; Sagnes, I.; Harouri, A.; Lanco, L.; Senellart, P.; Eisenberg, H. S. Sequential Generation of Linear Cluster States from a Single Photon Emitter. *Nature Communications* **2020**, *11*, 5501.

(43) Ballesteros, G.; Proux, R.; Bonato, C.; Gerardot, B. readPTU: A Python Library to Analyse Time Tagged Time Resolved Data. *J. Instrum.* **2019**, *14*, T06011.

(44) de la Peña, F.; Prestat, E.; Fauske, V. T.; Burdet, P.; Furnival, T.; Jokubauskas, P.; Lähnemann, J.; Nord, M. hyperspy/hyperspy: Release v1.6.4. *https://doi.org/10.5281/zenodo.5608741*